type TiO_2 boundary (*17*) can be used to determine the pressure and temperature of the rock in the diamond stability field. In the present case, the subduction limit is close to the graphite-diamond boundary, but it may be different in other cases because of different temperature conditions and the envelope shape of the rutile–α-PbO_2 phase boundary. The baddeleyite/α-PbO_2–type TiO_2 boundary (*22*) could be a useful indicator of possible subduction to the transition zone of the mantle if baddeleyite-type TiO_2 can be preserved in a host of minerals with a high bulk modulus, such as diamond.

References and Notes

1. J. G. Liou, R. Y. Zhang, W. G. Ernst, D. Rumble III, S. Maruyama, *Rev. Mineral.* **37**, 33 (1998).
2. C. Chopin, *Contrib. Mineral. Petrol.* **86**, 107 (1984).
3. N. V. Sobolev and V. S. Shatsky, *Nature* **343**, 742 (1990).
4. H. J. Massonne *et al.*, *Eur. J. Mineral.* **10**, 497 (1998).
5. S. Xu *et al.*, *Science* **256**, 80 (1992).
6. L. F. Dobrzhinetskaya *et al.*, *Geology* **23**, 597 (1995).
7. H. J. Massonne, in *Proceedings of the 7th International Kimberlite Conference* (Cape Town, South Africa, April 1998), in press. The *P-T* conditions of three different stages of metamorphism of the quartzofeldspathic rocks from the Saxonian Erzgebirge were derived on the basis of the chemical zonation of garnet and phengite. The first stage is characterized by pressure conditions around 2 GPa at temperatures of about 700°C. The second stage is characterized by burial of the diamondiferous gneisses to depths of at least 130 km, which is suitable for diamond formation. Temperature between 900° and 1000°C were reached, as evidenced by introduction of Ti in the garnet. (A semiquantitative approach to metamorphic temperatures was taken using the Ti contents in Al-garnet coexisting with rutile and a SiO_2 phase. To ensure that he had plausible temperatures, Massonne compared his estimated data to metamorphic temperatures from the literature for the range from 600° to 1400° C.) Subsequent exhumation of the diamondiferous gneisses was accompanied by cooling. During this process, microdiamonds were enclosed in garnet before they could be completely graphitized. The third stage was characterized by phengite formation at temperatures around 750°C and pressures between 2 and 1.5 GPa.
8. A. Kriner and A. P. Willner, *Mineral. Petrol.* **132**, 1 (1998).
9. We used a JEOL 3010 instrument at 300 keV for imaging, electron diffraction, and point-count EDX of the argon-ion milled thin foils, which were supported by a molybdenum grid and a copper ring. To diminish beam-spreading effects, we used the smallest size (5 nm) and highest energy (300 keV) of the electron beam available with this instrument for EDX analysis at the thin area (<200 nm thick) of the specimen. Under such conditions, the x-ray spatial resolution was calculated to be 12 nm according to the single-scattering model [see D. B. Williams and C. B. Carter, *Transmission Electron Microscopy—Spectrometry IV* (Plenum, New York, 1996), p. 623; S. J. B. Reed, *Ultramicroscopy* **7**, 405 (1982)]. Therefore, with the α-PbO_2–structured TiO_2 slab (8 nm thick) edge-on, there was likely a considerable volume fraction of the slab analyzed out of total TiO_2 (i.e., α-PbO_2–structured TiO_2 slab plus rutile).
10. The angles between zone-axis patterns read from a Wulff net plotted with the double tilting angles of the AEM specimen holder are 19.5° ± 0.5° for [110]/[210], 8.5° ± 0.5° for [210]/[310], and 21.5° ± 0.5° for [310]/[100], in close agreement with the angles 19.2°, 9.1°, and 21.8°, respectively, calculated from the lattice parameters and orthorhombic indices of synthetic α-PbO_2–structured TiO_2 (*11*).
11. P. Y. Simons and F. Dachille, *Acta Crystallogr.* **23**, 334 (1967).
12. B. G. Hyde and S. Andersson, *Inorganic Crystal Structures* (Wiley, New York, 1989), pp. 67–72.
13. The eight *d*-spacings measured from Fig. 2 and compiled in Table 1 were used for least-squares refinement of the lattice parameters. The error of the *d*-spacing measurements on SAED patterns taken at a camera length of 150 cm and with rutile reflections in the same negatives as standard was estimated to be ±0.002 nm.
14. For example, 010 and 011 (actually 01*l*) diffractions are forbidden, as shown in Fig. 2D. Other systematic absences, such as 001 and 120, were confirmed by tilting to a systematic row of spots to avoid double diffractions. The nonforbidden spots were also confirmed in this way.
15. See T. Hahn (Ed.), *International Tables for Crystallography, Vol. A, Space Group Symmetry* (Reidel, Dordrecht, Netherlands, 1987), pp. 190–321.
16. K. Kusaba, M. Kikuchi, K. Fukuoka, Y. Syono, *Phys. Chem. Miner.* **15**, 238 (1988).
17. J. S. Olsen, L. Gerward, J. Z. Jiang, *J. Phys. Chem. Solids* **60**, 229 (1999). This phase boundary was recently determined by in situ x-ray powder diffraction using a synchrotron radiation source during heating and compression experiments in the multianvil device for bulk and nanophase material. When plotted in a *P-T* diagram, the rutile/α-PbO_2–type TiO_2 phase boundary changes from a negative to a positive slope with increasing temperature at ~6 GPa and 850°C for bulk material and at ~4 GPa and 900°C for nanophase material. The topology of the TiO_2 phase diagram is so similar to that of iron that the slope change of the phase boundary may be due to entropy change in either the rutile or the α-PbO_2–type phase, analogous to spin ordering at Curie transition for the iron phase with body-centered cubic structure. The curvature and change of slope went undetected in an earlier study [M. Akaogi *et al.*, in *Program and Abstracts of Papers Presented at the 30th High-Pressure Conference of Japan*, Y. Syono, Ed. (Japan Society of High Pressure Science and Technology, Kyoto, 1989), p. 111 (in Japanese)], possibly because of sluggishness of the transition at temperatures lower than 800°C.
18. Thermodynamically, the surface energy contribution to the energetics of a solid-solid transformation increases with decreasing crystal size. Because the size dependence of surface energy is different for different phases, the change in transition pressure with crystal size can be either way, depending on the system under investigation (*17*). In the case of CdSe, the transition from a wurtzite to a rock salt structure takes place at a higher pressure for nanocrystals than for the bulk [see S. H. Tolbert and A. P. Alivisatos, *Science* **265**, 373 (1994)]. As for the case of titania, the transformation pressure is lower for nanophase material than for the bulk, although the underlying mechanism has yet to be clarified (*17*).
19. R. G. Berman, in *The Properties of Diamond*, J. E. Field, Ed. (Academic Press, London, 1979), pp. 4–22.
20. A. N. Winchell and H. Winchell, *Elements of Optical Mineralogy—An Introduction to Microscopic Petrography* (Wiley, New York, ed. 4, 1961), p. 66.
21. D. G. Issak, J. D. Carnes, O. L. Anderson, H. Cynn, E. Hake, *Phys. Chem. Miner.* **26**, 31 (1998).
22. J. Tang and S. Endo, *J. Am. Ceram. Soc.* **76**, 796 (1993).

23. We thank H. J. Massonne for supplying the diamondiferous gneiss sample and unpublished results, L. J. Wang for her technical assistance on AEM, and referees for constructive comments. Supported by National Science Council, Taiwan, ROC (S.-L.H., P.S.).

17 February 2000; accepted 2 March 2000

The Influence of Canadian Forest Fires on Pollutant Concentrations in the United States

Gerhard Wotawa[1]*† and Michael Trainer[2]

High carbon monoxide (CO) concentrations from uncertain origins occurred episodically in the southeastern United States during the summer of 1995. We show that these episodes were caused by large forest fires in Canada. Over a period of 2 weeks, these natural emissions increased CO concentrations in the southeastern United States as well as along the eastern seaboard, a region with one of the world's highest rates of anthropogenic emissions. Within the forest fire plumes, there were also high concentrations of ozone, volatile organic compounds, and aerosols. These results suggest that the impact of boreal forest fire emissions on air quality in the mid-latitudes of the Northern Hemisphere, where anthropogenic pollutant sources have been considered predominant, needs to be reevaluated.

Forest fires are known to be a major source of CO and other air pollutants on a global scale (*1*). Large forest fire plumes, however, have been found mostly in tropical regions and above the oceans (*2*, *3*). A number of studies dealing with the influence of fires in boreal forests on trace gas concentrations in high northern latitudes were conducted as part of the NASA Arctic Boundary Layer Expeditions (*4*, *5*). It was shown that summertime sub-Arctic haze events were primarily a result of forest fires (*6*), that fires, together with stratospheric intrusions, contribute a major fraction of total oxidized nitrogen species (NO_y) in the remote sub-Arctic troposphere (*7*), and that these fires provide a net source

[1]University of Agricultural Sciences, Institute for Meteorology and Physics, Tuerkenschanzstrasse 18, A-1180 Vienna, Austria. [2]National Oceanic and Atmospheric Administration (NOAA) Aeronomy Laboratory, 325 Broadway, Boulder, CO 80303, USA.

*Visiting scientist at CIRES, University of Colorado, and NOAA Aeronomy Laboratory.

†To whom correspondence should be addressed. E-mail: gerhard.wotawa@boku.ac.at

of CO and volatile organic compounds (VOCs) into the mid-latitudes (*8*). Specific studies dealing with boreal forest fire emissions in northern Canada indicate that high CO emissions can be expected from high-intensity crown fires there (*9*). Recent measurements in Siberia also exhibited elevated CO levels across a large area as a result of burning (*10*, *11*). However, the influence of such fires on CO concentrations measured at mid-latitude monitoring sites has not been quantified before.

In the summer of 1995, a field measurement campaign (SOS95) was conducted in central Tennessee as part of the Southern Oxidants Study (*12*). During this campaign, episodes of high CO concentrations that could not be attributed to anthropogenic activity occurred simultaneously at all level-II (*13*) ground sites. Using ground measurements, aircraft measurements, and model simulations, we show that these episodes were caused by forest fires in Canada (*14*) before and during the campaign period and demonstrate how natural emissions from forest fires strongly influenced CO concentrations in the southeastern and eastern United States during a period of 2 weeks. These plumes were transported across more than 3500 km. They also contained high concentrations of ozone (O_3), VOCs, and aerosols.

On the basis of CO measurements at four background stations in the SOS95 region (*15*) and two background stations in the eastern United States (*16*), we statistically reconstructed CO source regions causing the measured variations. For this purpose, backward air trajectories ending at these stations were calculated (*17*) with the FLEXTRA trajectory model (*18*) based on meteorological analysis data contributed by the European Centre for Medium-Range Weather Forecasts (ECMWF) (*19*). A method of trajectory statistics (*20*), the redistributed concentration field method (*21*), was applied on CO measurements and corresponding trajectories. Besides the expected anthropogenic CO source regions, our statistics indicated the existence of even stronger emission sources in northwestern Canada (see Fig. 1). This is unusual, because previous studies showed that CO concentrations in the eastern United States are normally lower when trajectories arrive from the far northwest (*22*). The main fire spot during June 1995, located in the Northwest Territories (*23*), was well identified by the statistics, together with other known fire locations (*24*). The results also indicate that CO emission strengths from forest fires exceeded those from anthropogenic sources.

Model simulations of CO transport from forest fires and from anthropogenic sources were performed by applying the particle diffusion model FLEXPART (*25*) to the ECMWF wind field analyses. Because of the long lifetime of CO, the simulations were carried out without considering chemistry or deposition. The simulation period was 17 June to 13 July 1995 (*26*). For the simulation of CO transport from Canadian forest fires, five emission areas were identified (*27*). To each of these regions, we attributed the area burned in the respective province (*28*) during the simulation period. CO emissions were assumed to be proportional to the burned area. A measurement-based estimate for the Northwest Territories suggests a CO emission of 4250 ± 425 kg per ha of burned forest (*9*). On the basis of this estimate, we assumed an emission of 4500 kg of CO per ha of forest. In total, about 1.2×10^{10} kg of CO was assumed to be emitted from the forest fires in the given time period. For the simulation of transport from anthropogenic CO sources, we made use of an emission inventory for 1996 on a U.S. county basis (*29*). For Canada, we used an inventory with base year 1985 (*30*). In total, 0.65×10^{10} kg of CO were assumed to be emitted from anthropogenic sources during the simulation period, which implies that the estimated total emissions from forest fires exceeded the estimated emissions from anthropogenic sources by a factor of two. In the model simulation, anthropogenic emissions were released between the surface and 300 m, and forest fire emissions between 500 and 3000 m, both equally distributed between minimum and maximum emission height. The elevated emission heights for forest fire emissions were selected to account for both the buoyancy of the emitted gases and the convection above the fire spots. Elevated effective emission heights from forest fires are documented in literature (*6*, *31*)

During the SOS95 campaign, the model calculated three episodes of large forest fire CO plumes. The major plume was transported behind a cold front on 1 July 1995 (Fig. 2), covering large parts of the central and southeastern United States. According to the model, other CO plumes passed by the end of June and 7 to 10 July. These simulations were validated by comparing them with surface measurements in the SOS95 region and on the East Coast. For this comparison, a summertime background CO concentration of 70 parts per billion (ppb) (*32*, *33*) was added to the modeled contributions from anthropogenic sources and from fires.

As a result, it turned out that forest fire emissions are needed to explain the observed time series of CO. At Giles County, Tennessee, only 3% of the variance of the average afternoon (18 to 21 UTC) CO concentrations can be explained by nonlocal anthropogenic influence, 74% by forest fire influence, and 90% by a combination of both sources (see Fig. 3). Similar results were also obtained for other SOS95 ground stations (Table 1). Looking at the afternoon CO concentrations at all sites together, transport from the forest fires explained between 52 and 74% of the variance of the afternoon CO concentrations. Long-range transport from anthropogenic sources explained only 0 to 6% of the variance during this episode. Thus, it can be concluded that, besides some local influence not accounted for, measured CO concentrations at the SOS95 ground measurement locations were dominantly influenced by Canadian forest fires during these 2 weeks.

Similar results showing the high influence of forest fire emissions on CO measurements were obtained for four sites at

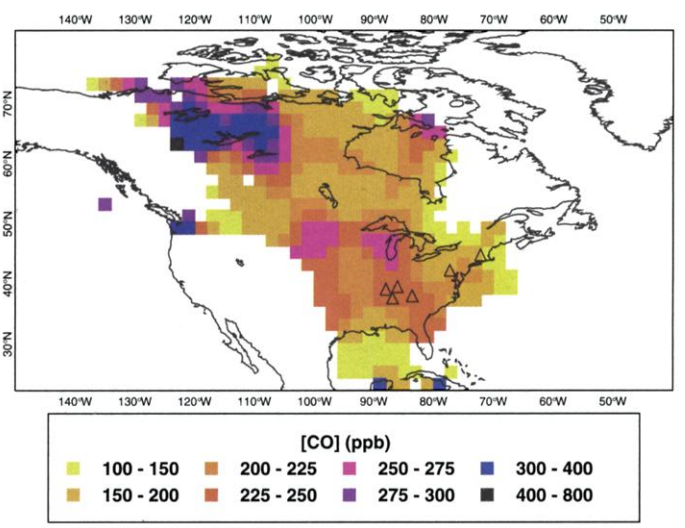

Fig. 1. Emission field of CO (in ppb) as reconstructed by the trajectory statistics (redistributed concentration field method) during the summer of 1995. Measurement sites are indicated by triangles. Data from the Wye River (MD) and Shenandoah (VA) stations are not included in this analysis. Regions with insufficient trajectory coverage are left blank. The principle of the statistics is to attribute measured pollutant concentrations to grid cells crossed by the respective trajectories. Afterward, an average, residence-time weighted concentration was computed for every cell. A high concentration value indicates the existence of a substantial source of the measured quantity within the cell.

the U.S. East Coast (Harvard Forest, MA; Arendtsville, PA; Wye River, MD; Shenandoah, VA), although the situation was more difficult to interpret. Forest fire influence there was not confined to well-defined episodes but persisted during much of the simulation period. Despite this, the percentage of explained variance by long-range transport from the fires ranged between 52 and 64% (Table 1) and again exceeded the percentage of variance explained by the simulation of transport from anthropogenic sources. The unexplained variance, coming probably from local influence, was higher at some of these sites.

For the SOS95 region, we observed no pronounced bias between model simulation and measurements. This absence of bias provides a strong confirmation of the large-scale validity of the Northwest Territory forest fire emission measurements (*9*). The model simulation, however, showed an overestimate of 33% at the four East Coast sites. But this bias could not be attributed to the forest fire simulation (*34*).

Table 1. Comparison between modeled and measured CO concentrations at different sites, with C_{meas} being the average measured concentration, C_{mod} the average modeled concentration, $C_{a,meas}$ the average measured afternoon (18 to 21 UTC) concentration, and $C_{a,mod}$ the average modeled afternoon concentration (all in ppb). r_a is the correlation coefficient of measured versus simulated daily afternoon concentrations only from anthropogenic sources, r_f is that only from forest fires, and r_b is that from both sources. The first four stations are SOS95 sites; the others are NARSTO (North American Research Strategy for Atmospheric Ozone) sites near the East Coast. The investigation period was 25 June to 10 July 1995.

	No.	C_{meas}	C_{mod}	$C_{a,meas}$	$C_{a,mod}$	r_a	r_f	r_b
			SOS sites					
Giles County, TN	13	231	231	225	213	0.18	0.86	0.95
Cove Mountain, TN	12	219	235	223	226	0.25	0.72	0.77
Mammoth Cave, KY	15	237	242	237	228	0.00	0.73	0.70
Land between the Lakes, KY	14	230	241	226	244	0.00	0.77	0.81
			East Coast sites					
Arendtsville, PA	8	188	288	173	280	0.46	0.80	0.80
Harvard Forest, MA	5	174	207	170	225	0.71	0.72	0.92
Wye River, MD	8	172	225	173	186	0.41	0.79	0.70
Shenandoah, VA	9	219	283	204	261	−0.25	0.73	0.47

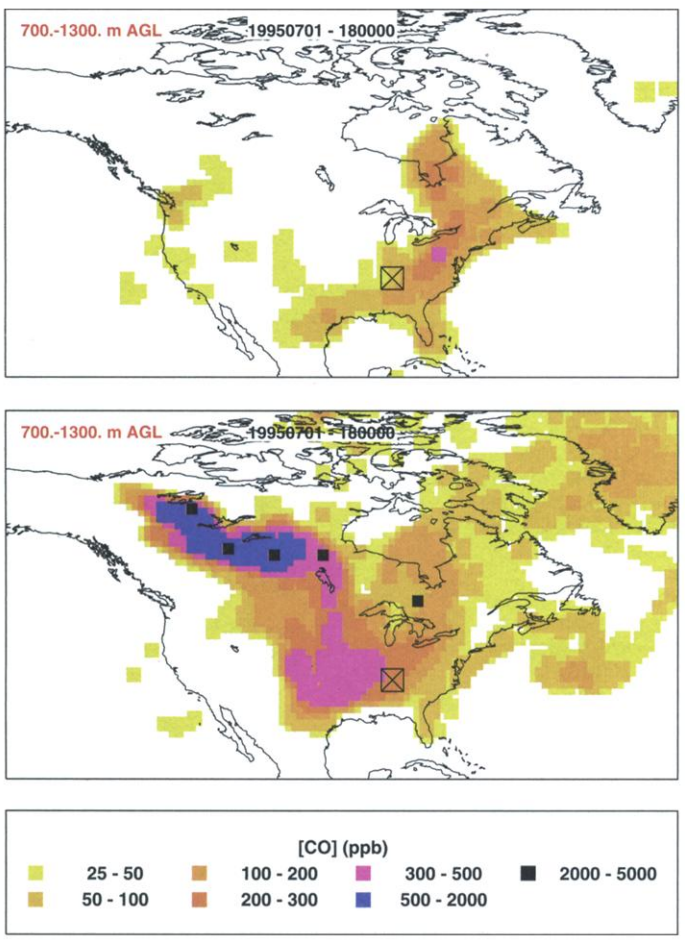

Fig. 2. Calculated CO concentrations (in ppb) from anthropogenic emissions (top) and from forest fires (bottom) for 1 July 1995, 18 UTC. Forest fire release locations are marked with black filled squares; the SOS95 Middle Tennessee study region is indicated by an open square. The anthropogenic concentrations are high ahead of a cold front crossing the southeastern and eastern United States, whereas forest fire concentrations are high behind the cold front. AGL, above ground level.

No high correlation coefficient between measured O_3 surface concentrations and calculated forest fire CO concentrations was found. Forest fire CO plumes were transported behind cold fronts, and the lower temperatures and the faster dilution of anthropogenic pollutants normally do not provide an environment favorable for local or regional photochemical O_3 production. However, the correlation between daily average O_3 and forest fire CO concentrations amounted to 0.46 (Giles County) and was significantly different from zero. Regional background O_3 concentrations were elevated by 10 to 20 ppb (*13*) on the two SOS95 intensive observation days (2 and 8 July) within the major forest fire episodes, compared with other days.

Forest fires changed the photochemical property of the air mass, as measured by the ratios of O_3 to NO_y and O_3 to CO. Measurements in Giles County showed that the correlation coefficient between O_3 and NO_y concentrations decreased from 0.91 to 0.67, the ozone production efficiency (slope of the regression line) dropped from 6.5 to 3.7 on days with strong forest fire influence, and the slope of O_3 versus CO dropped from 0.20 to 0.05. The first value is typical for summertime conditions in North America (*35*); the second can be explained by a combination of O_3 deposition during the transport toward the station and lower NO_x to CO emission ratios in the fires, consistent with results from previous studies (*7*, *36*, *37*).

From the SOS95 aircraft measurements as well as from model simulations, a lot can be learned about the properties of the boreal forest fire plumes reaching the midlatitudes. These plumes are transported behind cold fronts within subsiding air masses. The transport height decreases with increasing transport time. During the flights, the influence of forest fire plumes could be detected between the surface and 3000 m above the ground, whereas studies in the sub-Arctic region identified plumes in heights up to 4500 m. Although forest fire plumes were always well defined with respect to CO, they gradually lost their definition with respect to O_3 after being integrated in the boundary layer (dry deposition). The amount of O_3 being transported from these plumes directly toward surface measurement sites thus depended on when and where these plumes reached the ground. Elevated plumes were always marked by enhanced O_3 concentrations. For instance, the elevated plume encountered

during the flight on 10 July above Indiana and Illinois showed O_3 values of 80 to 100 ppb over a tropospheric background of 50 ppb (Fig. 4). The observed O_3 versus CO ratio (0.11) suggests, well in accordance with other studies (*36*, *37*), a reduced O_3 enhancement with respect to CO within forest fire plumes, compared with plumes from cities. However, fire plumes provide an enhanced background on which local-scale as well as regional-scale anthropogenic O_3 episodes can build up. Photochemical model simulations indicate that excess O_3 concentrations of tens of ppb can be expected over the eastern and southeastern United States as a result of the forest fires. In addition to the O_3 enhancement, aircraft measurements showed increased concentrations of VOCs and particulate matter within these plumes.

Using the emission estimate confirmed by our model results and combining it with the Canadian forest fire statistics (*28*), the contribution of Canadian forest fire CO emissions can be compared with the CO emissions of the United States (*29*), amounting to about 8.15×10^{10} kg/year. On the basis of the forest area burned in Canada annually on the 10-year average (3×10^6 ha), we estimate that these sources amount to 17% of the U.S. CO emissions. In 1995, the forest fire CO emissions in Canada amounted to 36% of the total U.S. emissions annually and to 280% during June 1995. Emission estimates of total nonmethane volatile organic compounds (NMVOC) emitted by Canadian forest fires (*9*) suggest that the contributions of Canadian forest fires to NMVOC concentrations in the southeastern and eastern United States during the summer of 1995 should have also been substantial. With these results, we extend the conclusion already drawn in a previous study (*8*). Boreal forest fires provide a substantial source of CO (and presumably also VOCs) into the mid-latitudes. Episodically, CO emissions from boreal fires are the dominant source of regional levels of CO for the eastern and southeastern United States, one of the highest emission regions worldwide.

The SOS95 measurements together with first photochemical model results indicate that forest fires influenced the build-up of ozone episodes in the southeastern United States by increasing background air pollution after passages of cold fronts that normally would clean the atmosphere. High O_3 concentrations were observed within these large plumes. Enhanced O_3 concentrations from the 1995 Canadian forest fires were also reported from a location closer to one fire spot (*38*). We therefore have to wonder whether tropospheric ozone pollution in the United States and elsewhere in the midlatitudes is, at least episodically, more influenced by these natural sources than currently believed and whether ozone reduction scenario calculations should account for these additional sources in the future.

These results are also relevant in the context of climate change. The number of forest fires in Canada has increased from 6000 annually during the 1930–1960 period to 10,000 in the 1980s (*39*). The area burned increased correspondingly. Although most of the Canadian fires can be attributed to human activity, 85% of the area burned is caused by lightning (*39*). The subsequent transport of forest fire plumes toward the United States is not uncommon. A recent study demonstrated close links between circulation anomalies in the midtroposphere and area burned in Canada (*40*). It was shown that in years such as 1995 with high forest fire activity in the west-central regions of Canada, there was typically a persistent high-pressure system located above northwestern Canada and the northern Pacific and a low-pressure system above northeastern Canada. Between these systems, transport of Canadian forest fire emissions toward the United States can take place. Situations similar to the 1995 case were observed in 1981, 1989, and 1994 (*40*).

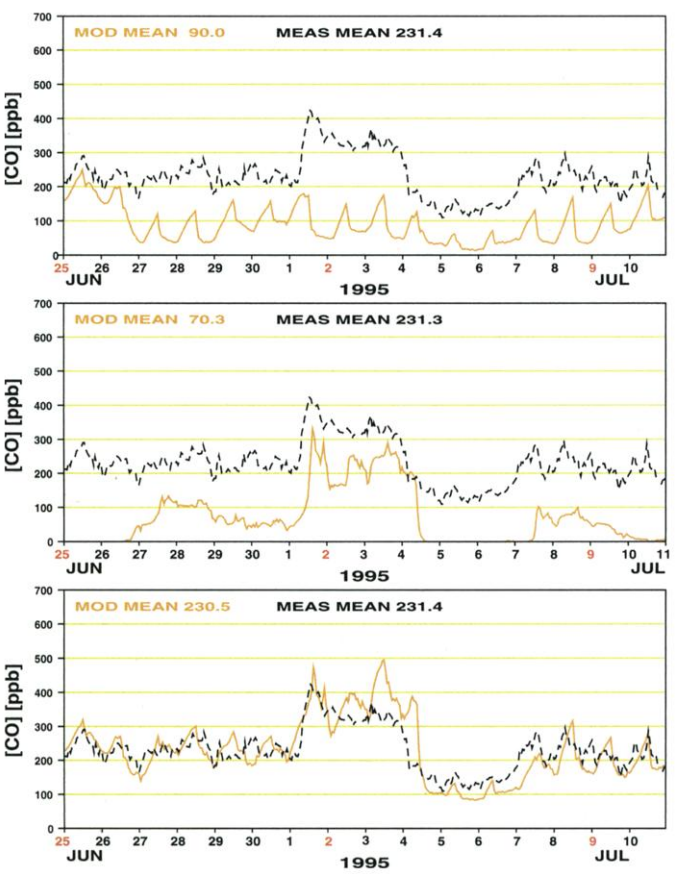

Fig. 3. Hourly values of measured CO (dashed line) and simulated CO (solid line) concentrations (in ppb) from anthropogenic sources (top), from forest fires (middle), and from both sources plus background (bottom) at station Giles County, Tennessee. The background concentration was taken as 70 ppb.

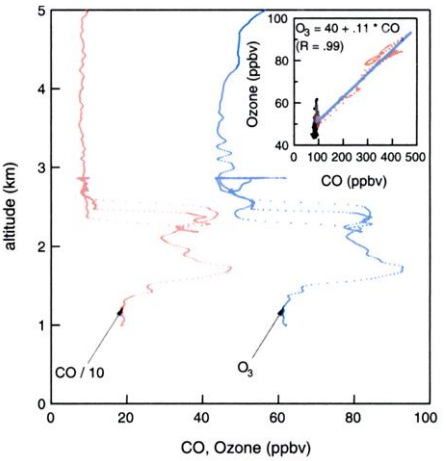

Fig. 4. Vertical distribution of CO (in ppb) and O_3 (in ppb) as measured by the aircraft on the afternoon of 10 July above the border between Indiana and Illinois (between 87° and 88°W along 39.7°N). The forest fire plume is marked by increased CO as well as by increased ozone concentrations. The aircraft probed the haze layer three times in a time span of 15 min, covering a distance of 55 km. The vertical extent of the layer varied somehow along this flight leg. The data for the O_3 to CO correlation and slope calculation are vertically restricted below 2600 m (red points in the scatter diagram) to avoid introducing an O_3 peak at 3 km of probably stratospheric origin (black points). All data represent 1S averages smoothed over 11 s.

References and Notes

1. P. J. Crutzen and M. O. Andreae, *Science* **250**, 1669 (1990).
2. I. Jonquieres, A. Marenco, A. Maalej, F. Rohrer, *J. Geophys. Res.* **103**, 19059 (1998).
3. C. E. Watson, J. Fishman, H. G. Reichle, *J. Geophys. Res.* **95**, 16443 (1990).
4. R. C. Harriss *et al.*, *J. Geophys. Res.* **97**, 16383 (1992).
5. R. C. Harriss *et al.*, *J. Geophys. Res.* **99**, 1635 (1994).
6. R. C. Harriss *et al.*, *J. Geophys. Res.* **97**, 16589 (1992).
7. S. C. Wofsy *et al.*, *J. Geophys. Res.* **97**, 16731 (1992).
8. S. C. Wofsy *et al.*, *J. Geophys. Res.* **99**, 1887 (1994).
9. W. R. Cofer, E. L. Winstead, B. J. Stocks, J. G. Goldammer, D. R. Cahoon, *Geophys. Res. Lett.* **25**, 3919 (1998).
10. P. J. Crutzen *et al.*, *J. Atmos. Chem.* **29**, 179 (1998).
11. P. Bergamaschi *et al.*, *J. Geophys. Res.* **103**, 8227 (1998).
12. J. F. Meagher, E. B. Cowling, F. C. Fehsenfeld, W. J. Parkhurst, *J. Geophys. Res.* **103**, 22213 (1998).
13. K. J. Olszyna, W. J. Parkhurst, J. F. Meagher, *J. Geophys. Res.* **103**, 31143 (1998).
14. In the early summer of 1995, high forest fire activity occurred in northern Canada. 4.3 million ha burned during June, 2.5 million of which were in the Northwest Territories [National Forestry Database Program, Canadian Council of Forest Ministers (nfdp.ccfm.org/)].
15. Cove Mountain in eastern Tennessee (Great Smokey Mountains National Park), Giles County (150 km south of Nashville), Land between the Lakes (Tennessee Valley Authority reservation between Tennessee and Cumberland rivers, KY), and Mammoth Cave (Mammoth Cave National Park, KY). These stations cover an area of about 7700 km^2.
16. Harvard Forest, MA, and Arendtsville, PA.
17. We calculated three-dimensional backward trajectories every three hours, ending 30 m and 500 m above the measurement site. The calculation period was 20 June to 20 July 1995.
18. A. Stohl, G. Wotawa, P. Seibert, H. Kromp-Kolb, *J. Appl. Meteorol.* **34**, 2149 (1995).
19. User guide to ECMWF products Version 2.1. (European Centre for Medium-Range Weather Forecasts, Reading, UK, 1995).
20. The principle of trajectory statistics is to attribute measured pollutant concentrations to grid cells crossed by the corresponding trajectories (i.e., by trajectories ending at the site simultaneously with the measurements). Afterward, an average, residence-time weighted concentration is computed for every cell. High concentration values indicate the existence of a substantial source of the measured quantity within the cell.
21. A. Stohl, *Atmos. Environ.* **30**, 579 (1996).
22. J. L. Moody, J. W. Munger, A. H. Goldstein, D. J. Jacob, S. C. Wofsy, *J. Geophys. Res.* **103**, 13181 (1998).
23. The major fire area was located around 120°W and 65°N between Great Bear Lake and Great Slave Lake.
24. Large forest fires were also observed in Alberta, Saskatchewan, Manitoba, and Ontario [see Canadian Forest Service, Canada Centre for Remote Sensing, Fire Monitoring, Mapping and Modelling System (available at fms.nofc.cfs.nrcan.gc.ca/firem3/index.html)].
25. A. Stohl and D. J. Thomson, *Boundary Layer Meteorol.* **90**, 155 (1999).
26. The model resolution was 1° in longitude and latitude. The model domain covered more than one-third of the Northern Hemisphere (170° to 20°W) from the surface to the top of the atmosphere. The advection was calculated grid-free, and there was no numerical diffusion. Diffusion in the boundary layer was parameterized, and boundary layer heights were computed with Richardson number profiles. The concentration evaluation grid consisted of 10 boxes from the surface to 11 km, with the lowest box from surface to 150 m.
27. Area 1, Northwest Territories; area 2, Northeastern Alberta; area 3, northern central Saskatchewan; area 4, northern central Manitoba; and area 5, Ontario (James Bay).
28. National Forestry Database Program, Canadian Council of Forest Ministers (available at nfdp.ccfm.org/).
29. National Air Pollutant Emission Trends 1900–1996, *EPA Report EPA-454/R-97-011* (Environmental Protection Agency, Washington, DC, 1997).
30. The 1985 NAPAP emissions inventory (Version 2): Development of the annual data and modeler's tapes, *EPA Report EPA-600/7-89-012a* (Environmental Protection Agency, Washington, DC, 1989).
31. R. M. Banta *et al.*, *J. Appl. Meteorol.* **31**, 1328 (1992).
32. W. Seiler, H. Giehl, H. Ellis, *WMO Spec. Environ. Rep. 10* (1976).
33. P. C. Novelli, K. A. Masarie, P. M. Lang, *J. Geophys. Res.* **103**, 19015 (1998).
34. Model agreement with U.S. East Coast measurements improved if the anthropogenic emissions were reduced but deteriorated if the forest fire emissions were reduced.
35. M. Chin, D. J. Jacob, J. W. Munger, D. D. Parrish, B. G. Doddridge, *J. Geophys. Res.* **99**, 14565 (1994).
36. D. L. Mauzerall *et al.*, *J. Geophys. Res.* **101**, 4175 (1996).
37. D. J. Jacob *et al.*, *J. Geophys. Res.* **97**, 16421 (1992).
38. L. Cheng, K. M. McDonald, P. Angle, H. S. Sandhu, *Atmos. Environ.* **32**, 673 (1998).
39. M. G. Weber and B. J. Stocks, *Ambio* **27**, 545 (1998).
40. W. R. Skinner, B. J. Stocks, D. L. Martell, B. Bonsal, A. Shabbar, *Theor. Appl. Climatol.* **63**, 89 (1999).

41. This study was performed during a visit of the corresponding author to the NOAA Aeronomy Laboratory made possible by a grant provided by the Max Kade Foundation, New York. Surface CO, NO_y, and O_3 measurement data came from SOS95 and NARSTO sites. Airborne measurements were made by D. Parrish and J. Holloway. The modeling was based on data from the European Centre for Medium-Range Weather Forecasts, provided by A. Krieger from the University of Agricultural Sciences, Vienna, Austria. We are grateful to A. Stohl, Technical University of Munich, who developed the FLEXPART model and was always open for discussion of the results.

18 November 1999; accepted 23 February 2000

Nonrandom Extinction and the Loss of Evolutionary History

Andy Purvis,[1]* Paul-Michael Agapow,[1] John L. Gittleman,[2] Georgina M. Mace[3]

The hierarchical nature of phylogenies means that random extinction of species affects a smaller fraction of higher taxa, and so the total amount of evolutionary history lost may be comparatively slight. However, current extinction risk is not phylogenetically random. We show the potentially severe implications of the clumped nature of threat for the loss of biodiversity. An additional 120 avian and mammalian genera are at risk compared with the number predicted under random extinction. We estimate that the prospective extra loss of mammalian evolutionary history alone would be equivalent to losing a monotypic phylum.

Current and projected species extinction rates exceed geologically normal background rates by several orders of magnitude (*1*–*3*), indicating that we face an extinction episode equivalent to mass extinctions of the paleontological past. When biodiversity is measured by evolutionary history, expressed as the total length of all the branches in the tree of life, a surprisingly high proportion is likely to survive even a massive extinction episode. This is because most species have close relatives and thus contribute little to the total branch length: Whole clades are lost only when all their species go extinct, which is unlikely under an assumption of phylogenetically random extinction. However, historical extinctions and current extinction risk are often not randomly distributed among species. For example, the 85 mammalian species extinctions since 1600 include at least five members of the extinct family Nesophontidae (*4*, *5*), and the prevalence of current threat varies significantly among orders of mammals (*6*) and birds (*7*). This nonrandomness will result in the loss of more branch length and more higher taxa than predicted by random extinction (*8*). Here, we quantify how the clumping of extinction risk affects the amount of evolutionary history under threat in mammals and birds, using two measures of biodiversity: the number of higher taxa (genera) and the total phylogenetic branch length [commonly referred to as "phylogenetic diversity" (PD)] (*9*).

Nee and May (*10*) showed that surprisingly little PD is lost under even catastrophic extinction scenarios. In one of their simulations, 81% of the phylogenetic branch length remained even when only 5% of the species survived an extinction episode. Their simulations assumed that extinction was random—the "field of bullets" scenario—or could be optimized through management (so as to minimize loss of branch length) and indicated that the amount preserved would be influenced by the topology of the phylogenetic tree.

In principle, we can envisage two natural scenarios that would result in nonrandom distribution of extinction risk. First, any phylogenetic clumping of factors that promote risk would increase the chance of all species in polytypic taxa—and hence those taxa as a

[1]Department of Biology, Imperial College, Silwood Park, Ascot SL5 7PY, UK. [2]Department of Biology, Gilmer Hall, University of Virginia, Charlottesville, VA 22903, USA. [3]Institute of Zoology, The Zoological Society of London, Regent's Park, London NW1 4RY, UK.

*To whom correspondence should be addressed. E-mail: a.purvis@ic.ac.uk